

The birth of intermediate-mass black holes in primordial galaxies

Muhammad A. Latif,¹★ Sadegh Khochfar,² Dominik Schleicher,³ Daniel J. Whalen^{4,5}

¹Physics Department, College of Science, United Arab Emirates University, PO Box 15551, Al-Ain, UAE

²Institute for Astronomy, University of Edinburgh, Royal Observatory, Blackford Hill, Edinburgh EH9 3HJ, UK

³Astronomy Department, Universidad de Concepción, Barrio Universitario, Concepción, Chile

⁴Institute of Cosmology and Gravitation, University of Portsmouth, Portsmouth PO1 3FX, UK

⁵Ida Pfeiffer Professor, University of Vienna, Department of Astrophysics, Tuerkenschanzstrasse 17, 1180, Vienna, Austria

Accepted XXX. Received YYY; in original form ZZZ

ABSTRACT

The discovery of quasars at $z \gtrsim 7$ poses serious challenges because it is not known how $10^9 M_\odot$ black holes formed by this epoch. The leading candidates for the seeds of these quasars are $10^5 M_\odot$ direct-collapse black holes forming in atomically cooled haloes at $z \sim 15 - 20$. However, the Lyman-Werner (LW) UV backgrounds required to form such objects are extreme, $\gtrsim 10^4 J_{21}$, and may have been rare in the early universe. Here, we model the formation of Population III stars in moderate LW backgrounds of 100 and 500 J_{21} that were much more common at early times. We find that these backgrounds allow haloes to grow to a few $10^6 - 10^7 M_\odot$ and virial temperatures of nearly 10^4 K before collapsing but do not completely sterilize them of H_2 . At the onset of collapse, $Ly\alpha$ cooling dominates in the outer regions of the halo but H_2 cooling regulates the collapse of the core, at rates that are 10 - 50 times those in minihaloes because of higher virial temperatures. Supercharged H_2 cooling leads to the formation of 1800 - 2800 M_\odot primordial stars, with radiative feedback from the star halting accretion and setting its upper limit in mass. Such stars may lead to a population of less-massive, lower luminosity quasars that could be discovered by the *James Webb Space Telescope*, *Euclid* and the *Roman Space Telescope* in the coming decade.

Key words:

quasars: general — black hole physics — early universe — dark ages, reionization, first stars — galaxies: formation — galaxies: high-redshift

1 INTRODUCTION

The discovery of quasars at $z > 7$ (Mortlock et al. 2011; Wu et al. 2015; Bañados et al. 2018; Yang et al. 2020) poses significant challenges to current paradigms of structure formation because it is not fully understood how supermassive black holes (SMBHs) formed less than a Gyr after the Big Bang (Volonteri 2010; Haiman 2013; Latif & Ferrara 2016; Woods et al. 2019; Inayoshi et al. 2019). A number of origins have been proposed for high- z quasars such as the BHs of Population III (Pop III) stars at $z \sim 25$ ($10 - 500 M_\odot$; Madau et al. 2014; Volonteri et al. 2015), runaway stellar collisions in marginally-enriched haloes at $z \sim 15 - 20$ ($1000 - 4000 M_\odot$; Devecchi & Volonteri 2009; Sakurai et al. 2017; Reinoso et al. 2018; Boekholt et al. 2018), and direct-collapse black holes (DCBHs) in atomically-cooled haloes at $z \sim 15 - 20$ ($\sim 10^5 M_\odot$; Schleicher et al. 2013; Latif et al. 2013b; Regan et al. 2014; Smidt et al. 2018; Chon et al. 2018).

DCBHs form when primordial haloes grow to masses $\gtrsim 10^7 M_\odot$ and virial temperatures of $\sim 10^4$ K without having previously

formed a star because they are immersed in strong Lyman-Werner (LW) UV backgrounds that destroy their H_2 (e.g., Latif et al. 2014b; Agarwal & Khochfar 2015; Agarwal et al. 2019) or in supersonic baryon streaming flows that prevent star formation even if H_2 is present (Tseliakhovich & Hirata 2010; Stacy et al. 2011; Greif et al. 2011; Schauer et al. 2017). Temperatures of 10^4 K activate $Ly\alpha$ cooling that triggers rapid baryon collapse at up to $1 M_\odot \text{ yr}^{-1}$ (Wise et al. 2008; Regan & Haehnelt 2009). Stellar evolution calculations have shown that such flows can create stars with masses $\gtrsim 10^5 M_\odot$ that collapse to DCBHs via the general relativistic instability (Hosokawa et al. 2013; Umeda et al. 2016; Woods et al. 2017; Haemmerlé et al. 2018a,b). DCBHs are the leading candidates for the seeds of the first quasars because they form in dense environments in haloes that can retain their fuel supply even when it is heated by the BH (Whalen et al. 2004; Alvarez et al. 2009; Whalen & Fryer 2012; Johnson et al. 2013; Smith et al. 2018).

The accretion rates of $0.1 - 1 M_\odot \text{ yr}^{-1}$ required to build up $10^5 M_\odot$ stars can only be sustained by atomic cooling, not H_2 , and the LW backgrounds required for the complete extinction of H_2 in haloes are extreme, as much as a few $10^4 J_{21}$ where $J_{21} = 10^{-21} \text{ erg s}^{-1} \text{ cm}^{-2} \text{ Hz}^{-1} \text{ sr}^{-1}$ (Sugimura et al. 2014; Latif et al. 2015). But

★ E-mail: latifne@gmail.com

there is a growing body of work that suggests that supermassive stars can form even in the presence of minute amounts of H_2 shielded deep in the cores of haloes exposed to more modest LW fluxes. [Safranek-Shrader et al. \(2012\)](#) examined the collapse of a $3 \times 10^7 M_\odot$ halo in a LW background of $100 J_{21}$ and found that that cooling at its center was still governed by H_2 and produced a sink particle with a mass of $\sim 1100 M_\odot$. [Latif et al. \(2014c\)](#) also found that $100 - 10,000 M_\odot$ primordial stars could form in halos immersed in moderate LW fluxes (see also [Latif & Volonteri 2015](#)).

Until recently, simulations of baryon collapse in atomically-cooled haloes ignored radiative feedback from stars at their centers because stellar evolution models predicted that they were likely cool and red, and therefore not strong sources of ionizing UV flux capable of halting accretion onto the star (although pressure due to outflowing $\text{Ly}\alpha$ cooling radiation may could affect flows deep in the core of the halo; [Smith et al. 2017](#)). The first models to incorporate stellar feedback found it had little effect on the growth of the star on AU scales over times of a few years ([Luo et al. 2018](#); [Ardaneh et al. 2018](#)). [Chon et al. \(2018\)](#) and [Regan & Downes \(2018b\)](#) followed the collapse of haloes in LW backgrounds of $100 - 5000 J_{21}$ for a few hundred kyr and also found that radiation from stars did not suppress accretion. However, the presence of even small mass fractions of H_2 in haloes in LW backgrounds of these magnitudes can reduce infall rates by 1 - 2 orders of magnitude, down to $0.005 - 0.03 M_\odot \text{ yr}^{-1}$. Stars growing at the low end of this range have been found to become blue and hot in stellar evolution models, with ionizing UV fluxes that could at least partially quench accretion ([Haemmerlé et al. 2018a](#)). How such feedback governs the final masses of stars in these backgrounds is not yet known.

The original simulations of atomically-cooled haloes that proceeded from cosmological initial conditions did not exhibit fragmentation or the formation of dense clumps that could later become multiple massive stars (although see [Bromm & Loeb 2003](#)). Later studies at higher resolution revealed that atomically-cooled gas fragmented on AU scales but could only follow the evolution of the clumps for a few tens of years and could not determine if they later became stars or were subsumed by the disk at later times ([Becerra et al. 2015, 2018](#)). [Regan & Downes \(2018a,b\)](#) and [Chon et al. \(2018\)](#) studied fragmentation at somewhat lower resolutions out to a few hundred kyr and found that some clumps persisted for long times but could not determine their final fates. [Suazo et al. \(2019\)](#) followed the collapse of atomically cooled haloes at intermediate resolutions in moderate LW backgrounds for ~ 600 kyr, longer than previous studies but still well short of the collapse of the stars. Inflow rates lasting for the times required to actually form DCBHs have only recently been confirmed to occur in numerical simulations ([Latif et al. 2020](#); [Regan et al. 2020](#); [Patrick et al. 2020](#)). Although binary and multiple DCBH systems formed in all three studies, which holds important implications for the detection of DCBH mergers by the Laser Interferometer Space Antenna (LISA) in coming decades, they did not include radiation from the stars and may not ultimately be self-consistent.

Here, we investigate the prospect of massive BH seeds formation in primordial halos ranging in mass from $1.5 \times 10^6 M_\odot$ to $2.3 \times 10^7 M_\odot$ in LW backgrounds of $100 J_{21}$ and $500 J_{21}$, which were much more common in the primordial universe than those required for complete photodissociation of H_2 . Our simulations are evolved for up to ~ 900 kyr, approximately three times longer than in comparable studies, and include radiative feedback from the stars coupled to hydrodynamics and primordial gas chemistry. We describe our simulations in Section 2, present our results in Section 3, and conclude in Section 4.

2 NUMERICAL METHOD

Our simulations were performed with the Enzo adaptive mesh refinement (AMR) cosmology code ([Bryan et al. 2014](#)). We initialize our runs with cosmological initial conditions generated by MUSIC ([Hahn & Abel 2011](#)) at $z=150$ with cosmological parameters taken from Planck 2016 data: $\Omega_M = 0.308$, $\Omega_\Lambda = 0.691$, $\Omega_b = 0.0223$ and $h = 0.677$ ([Planck Collaboration et al. 2016](#)). Our simulation volume is $1 \text{ cMpc } h^{-1}$ on a side with a top grid resolution of 256^3 and two additional nested grids each with a resolution of 256^3 that span 20% of the top grid. We place the halo of interest at the center of the box and allow up to 16 additional levels of refinement during the runs to achieve resolutions of up to $\sim 300 \text{ AU}$. We split dark matter (DM) particles in this region into 13 child particles, which produces an effective DM resolution of $5 M_\odot/h$. Beginning at $z = 150$, we refine on Jeans length, baryonic overdensity and particle mass resolution, as in [Latif & Khochfar \(2020\)](#) and [Latif et al. \(2020\)](#). The Jeans length is resolved by at least 32 cells in our models.

We introduce sink particles that represent Pop III stars in cells where the maximum refinement level is reached, typically at densities of $\geq 10^{-16} \text{ g/cm}^3$. Our criteria for sink particle formation is based on SmartStars ([Regan & Downes 2018b](#)). A sink particle is allowed to form in a grid cell when meeting the following criteria: I) the grid cell is at the maximum refinement level; (II) the cell density is higher than the Jeans density; (III) the flow is convergent; (IV) the cooling time is shorter than the free-fall time; (V) the cell is at a local minimum of the gravitational potential. It can accrete gas from a radius of 4 cells and merges with the most massive particle within the accretion radius.

Stars are treated as red and cool if their accretion rates exceed $0.04 M_\odot \text{ yr}^{-1}$ and as hot and blue if they accrete below this rate. We assign a 10^5 K blackbody spectrum to blue stars ([Schaerer 2002](#)) and a 5500 K blackbody spectrum to red stars ([Hosokawa et al. 2013](#)), assuming in both cases that their luminosities scale with their masses. Photons from stars are propagated throughout the simulation volume with the MORAY raytracing radiation transport package, which is self-consistently coupled to hydrodynamics and non-equilibrium primordial gas chemistry in Enzo ([Wise & Abel 2011](#)). The flux is partitioned into five energy bins: 2.0 eV and 12.8 eV , which can destroy H^- , H_2 and H_2^+ , and three ionizing energies, 14.0 eV , 25.0 eV , 200.0 eV . We use SEDOP to populate the last three bins ([Mirocha et al. 2012](#)). Further details about sink particles and feedback can be found in [Regan & Downes \(2018b\)](#).

We employ a non-equilibrium primordial chemistry solver ([Abel et al. 1997](#)) to evolve the nine primordial species in our runs: H , H^+ , H^- , He , He^+ , He^{++} , H_2 , H_2^+ , e^- . Our simulations include H_2 cooling, collisional excitation and ionization cooling by H and He , bremsstrahlung cooling and recombinational cooling. Uniform LW backgrounds of 100 or $500 J_{21}$ are turned on at $z = 30$ to suppress star formation in minihaloes and self-shielding of H_2 is approximated by fits from [Wolcott-Green et al. \(2011\)](#). We ignore radiation pressure due to photoionizations, which could facilitate H II region breakout by imparting momentum to the surrounding gas. [Whalen & Norman \(2008\)](#) examined the impact of radiation pressure at lower densities and found that they amount to at most 20% of the ionized gas pressure. We therefore conclude that radiation pressure will not strongly affect our results.

3 RESULTS

We have simulated six halos, labelled H1, H2, H3, H4, H5 and H6, whose masses and collapse redshifts are listed in Table 1.

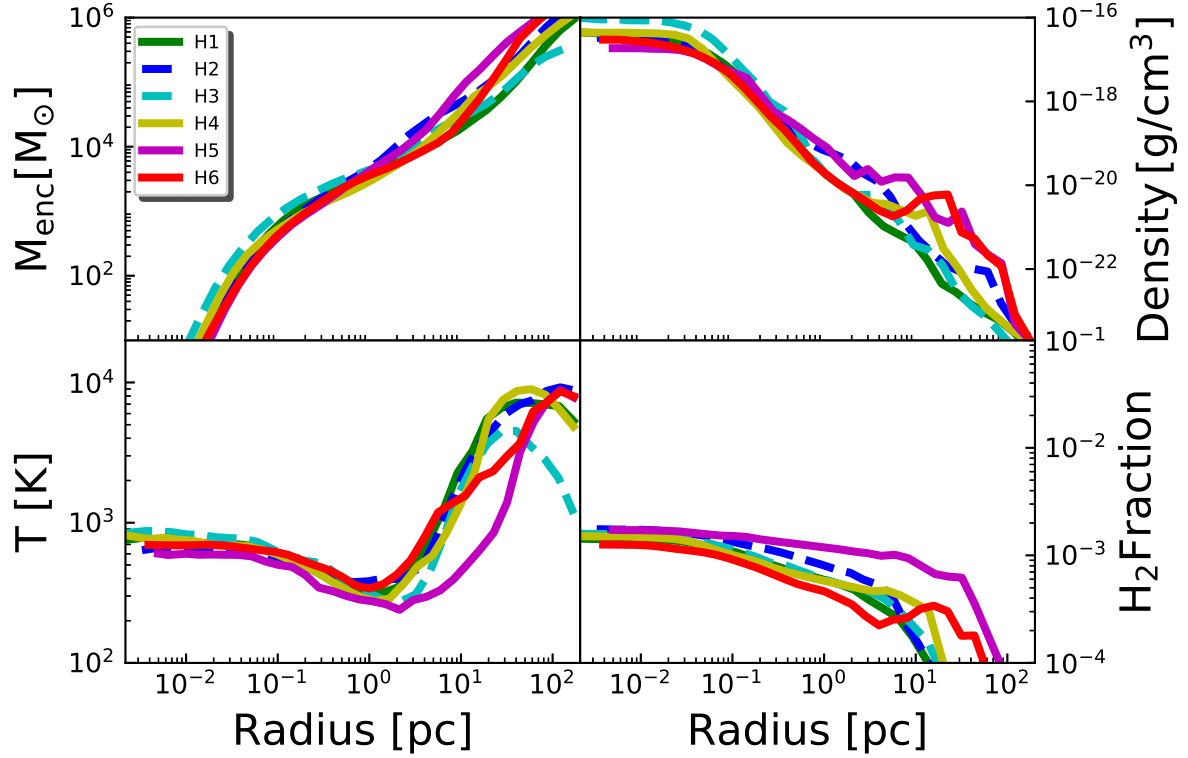


Figure 1. Spherically averaged radial profiles of density, temperature, enclosed mass and H_2 mass fraction at the onset of SF. Green, blue, cyan, yellow, magenta and red colors are haloes H1, H2, H3, H4, H5, and H6, respectively.

Table 1. Virial masses, collapse redshifts and LW backgrounds for the six haloes in our study. The final masses of the stars in each halo are listed in column 5.

Halo	z	Mass (M_\odot)	J_{21}	Stars (M_\odot)
H1	16.5	7.5×10^6	100	196, 97, 27, 2775
H2	14.5	2.3×10^7	500	1668, 10, 8683
H3	22.8	1.5×10^6	100	2743
H4	18.5	5.4×10^6	500	60, 94, 25, 2638
H5	13.3	1.3×10^7	100	346, 520, 1161, 2079
H6	13.31	1.7×10^7	500	546, 1955

3.1 Initial Collapse

Baryon collapse is suppressed by LW radiation in all six haloes until they reach masses of at least $10^6 M_\odot$, and in most cases $10^7 M_\odot$ (Latif & Khochfar 2019). However, as shown in the temperature profiles in Figure 1, once collapse begins it is mediated by both $\text{Ly}\alpha$ and H_2 cooling. At the onset of star formation (SF) atomic cooling dominates down to radii of a few pc, where gas is at temperatures of ~ 8000 K, but H_2 cooling, which produces temperatures of 300 - 1000 K, dominates at radii less than 1 pc. This can also be seen in the H_2 mass fractions, which can exceed 10^{-3} below 1 pc because they are self-shielded from the external background. The H_2 -cooled

core of the halo is at higher temperatures than those in normal Pop III star-forming haloes, which are typically 200 - 300 K, because they are subject to higher mass loading from atomic cooling in the surrounding gas. H5, which has the highest H_2 mass fraction, has the lowest temperatures and highest densities because of the larger cooling rates. Conversely, H6, which has the lowest H_2 mass fractions, has some of the lowest densities and highest temperatures.

The two-phase temperature structure in our haloes is due to the LW background, which allows them to grow to larger masses and higher virial temperatures before collapsing but does not completely sterilize them of H_2 . Because their cores are at higher temperatures than those of normal Pop III star-forming haloes, H_2 cooling and formation rates, which peak at 1000 - 2000 K, are much higher there (O’Shea & Norman 2007). This leads to central accretion rates that are much higher than those in normal minihaloes but less than those in isothermal atomically-cooled haloes in much higher LW backgrounds.

3.2 Disk Evolution / Star Formation

As shown in Figure 2, collapse leads to the formation of thick, rotationally flattened disks with initial radii of ~ 0.1 pc and masses of a few thousand solar masses. They grow to ~ 0.2 - 0.3 pc in radius by the end of the runs at nearly 1 Myr. These disks are a factor of five smaller in radius than those in isothermal atomically-cooled flows

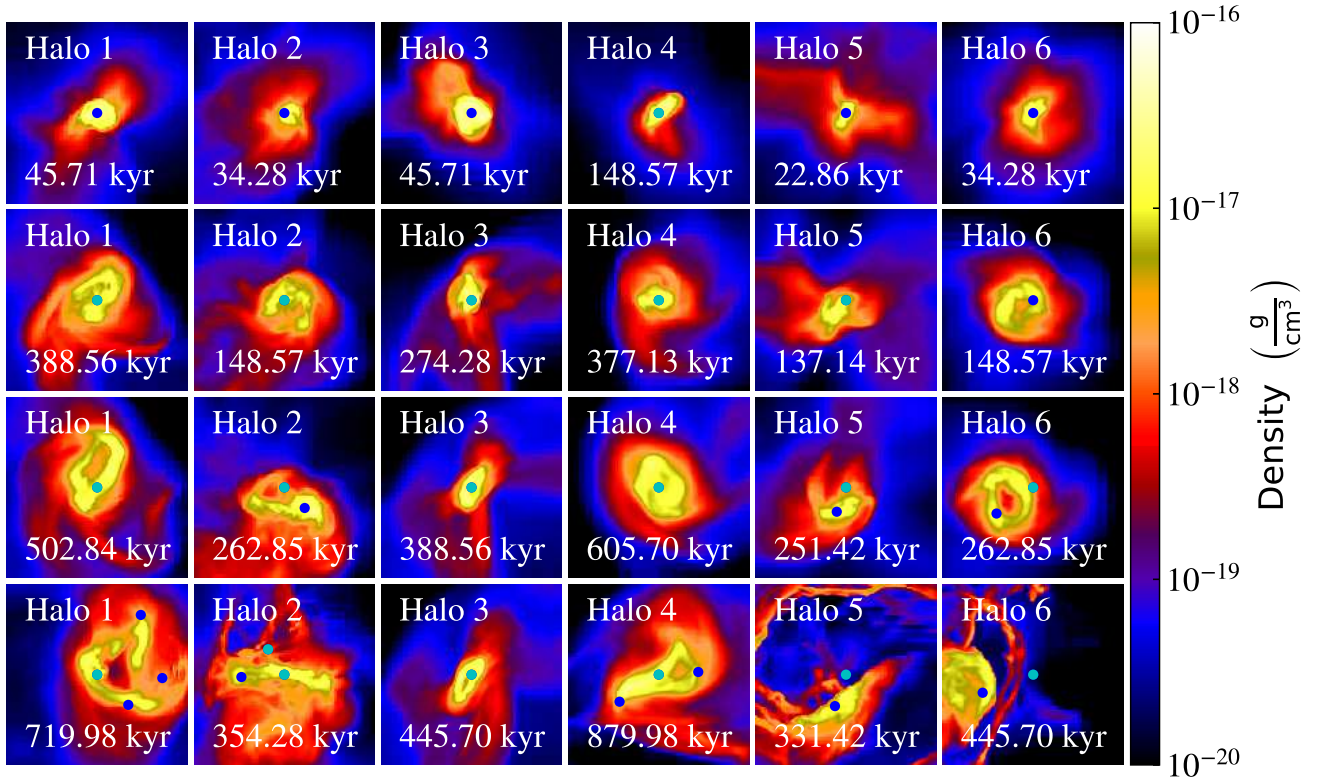


Figure 2. Disk evolution and SF in all six haloes. The images are density projections showing the average gas density along the line of sight and are 1 pc on a side. Dark blue dots are stars with masses $\geq 10 M_{\odot}$ and cyan dots are stars with masses $\geq 1000 M_{\odot}$. Each column shows the disk evolution in one halo.

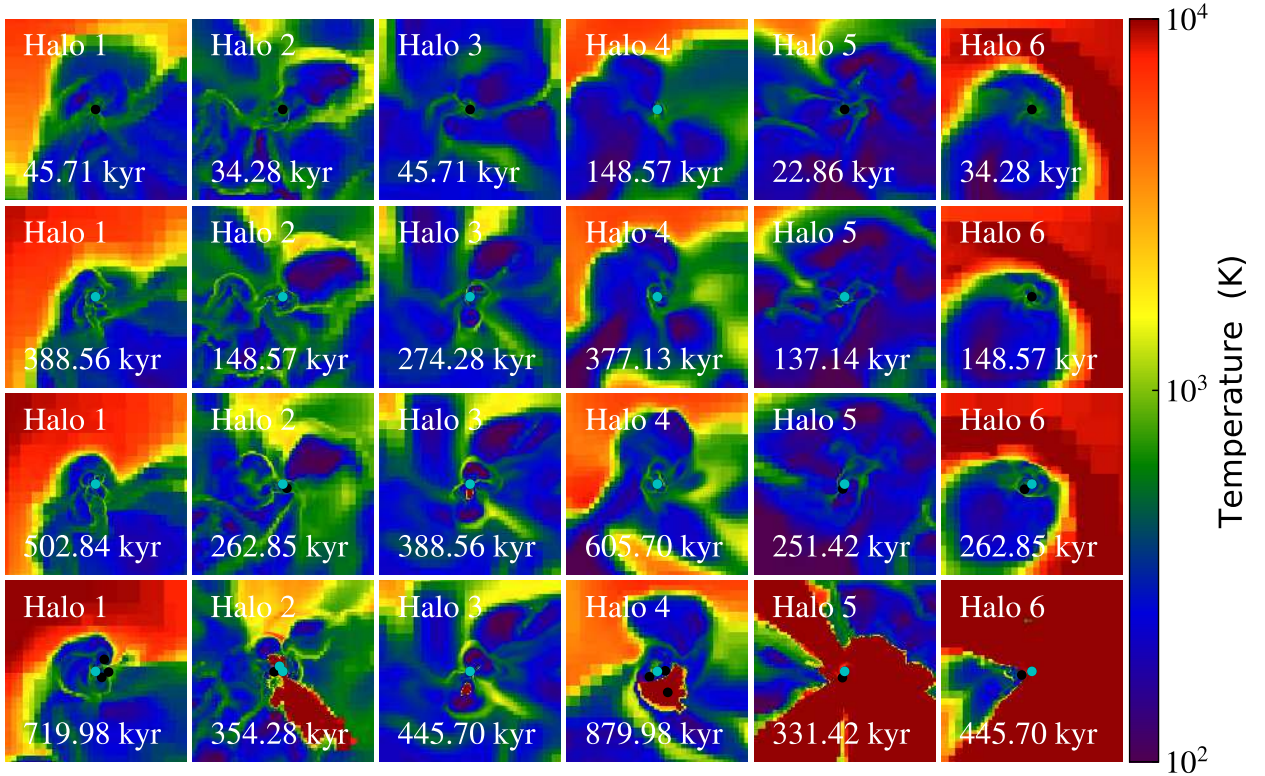


Figure 3. Temperature slices of the central 5 pc of the halo, taken along the x-axis.

at similar times because of lower infall rates due to less efficient H_2 cooling. At later times the disks develop irregular features created by gravitational torquing due to the formation of secondary stars and ionizing UV feedback from the stars, as we discuss in greater detail below.

A single star particle with a mass of a few solar masses forms first at the center of each disk when it reaches densities of $\sim 10^{-16} \text{ g cm}^{-3}$. Although new star particles can form within the accretion radius of this star at times and merge with it a few hundred or thousand years later, it mostly grows by accretion of dense gas. Secondary stars begin to appear by $\sim 250 \text{ kyr}$ in H2, H5 and H6, at 720 kyr in H1 and at 740 kyr in H4. At the end of the run H1, H4 and H5 host four stars, H2 has three and H6 has two. H3 forms a few low-mass stars but they are subsumed into the central star and only it remains at the end of the run at 900 kyr . Most of the additional stars have masses of a few tens to hundreds of solar masses, as shown in Table 1.

3.3 Radiative Feedback

Because accretion onto the main star begins at rates of a few $10^{-3} \text{ M}_\odot \text{ yr}^{-1}$ in all six haloes (on par with normal Pop III star-forming haloes; Latif et al. 2013c; Hosokawa et al. 2016), it is initially treated as a hot, blue source of ionizing photons. Recombination times in the vicinity of the stars are about 100 yr and they initially have low masses and luminosities so this UV flux remains trapped deep in the disk. However, at later times radiative feedback from the main star and gravitational torques from secondary stars clear gas from some of the disks, creating the annular structures and density gaps visible at 720 kyr in H1 and at 262.9 kyr in H6 (and even disrupting the disk, as shown at 354.3 kyr in H2.) Dynamical interactions with other stars can displace the main star into regions of lower density ($\sim 10^{-20} \text{ g cm}^{-3}$) where highly anisotropic H II regions can break out along lines of sight with lower column densities, as shown at 354.3 kyr in H2, 331.4 kyr in H5, and 445.7 kyr in H6 in Figure 3. I-front blowout evacuates gas from the vicinity of the star in these three haloes and terminates its growth. Three-body interactions also eject a secondary star from the center of the disk in H1 and H4.

To better quantify accretion in the midst of radiative outflows from the disks we plot spherically averaged mass inflow ($4\pi R^2 \rho v_{\text{rad}}^-$) and outflow ($4\pi R^2 \rho v_{\text{rad}}^+$) rates through radial shells in each halo in Figure 4. Inflow rates average $\sim 0.01 \text{ M}_\odot \text{ yr}^{-1}$ at 1 pc and fall to $10^{-4} \text{ M}_\odot \text{ yr}^{-1}$ in the vicinity of the main star. Outflows dominate inflows in H2, H5 and H6 due to I-front breakout from the disk. In H3 and H4, outflow rates exceed inflow rates at pc scales at later times. In general, outflow rates are either greater than or comparable to inflow rates within $\sim 1 \text{ pc}$ of the star in most of the haloes. They rise over time, can be quite intermittent, and vary from halo to halo. Inflow rates fall steeply in the central 0.2 pc of the disk so accretion onto the star is expected to be low at later times.

We show spherically averaged profiles of density, enclosed mass, temperature and H_2 mass fraction at the end of our simulations in Figure 5. Mean densities in the center of the halo have fallen by a factor of a few and the profile has become flattened in the central 0.5 pc because of gravitational torques and stellar feedback. In H5 and H6 densities have fallen by about six orders of magnitude where shocked ionized flows in the H II region of the star have driven gas out of the core of the halo. Average temperatures in this region have likewise risen above 10^4 K because of photoionizations and H_2 mass

fractions have fallen by a few orders in magnitude because it has been collisionally dissociated by free electrons. Average temperatures in the rest of the haloes are a few hundred Kelvin and H_2 abundances are a few 10^{-3} due to episodic recombination of ionized gas.

The small bumps in the H_2 profiles at $\sim 0.2 \text{ pc}$ and 0.4 pc in H5 and H6 are due to rapid H_2 formation in the outer layers of the I-front. The inclusion of multiple ionizing photon energies in the spectrum of the star leads to the broadening of the front, and its outer layers can fall to ionization fractions of 10% and gas temperatures of $1000 - 2000 \text{ K}$, which are prime conditions for H_2 formation in the gas phase via the H^- channel (Ricotti et al. 2001; Whalen & Norman 2008). The larger bumps in H_2 abundance at $\sim 1 \text{ pc}$ in H5 and H6 arise because the dense shell of gas swept up by the D-type I-front behind them partly shields them from LW radiation from the star. Approximately 1000 M_\odot of gas resides within the central 1 pc in all six haloes.

3.4 Accretion Rates / Final Stellar Masses

Masses and accretion rates for the main star and next most massive star in each halo are shown in Figure 6. Accretion rates begin at a few $10^{-3} \text{ M}_\odot \text{ yr}^{-1}$, rise to a few $10^{-2} \text{ M}_\odot \text{ yr}^{-1}$, and then fall by an order of magnitude as the stars grow in mass and luminosity. High densities, ram pressures, and short recombination times in the vicinity of the star confine its H II region close to its surface and allow accretion to proceed for a few hundred kyr in all six haloes. In H1, an H II region never develops and the star continues to accrete at a few $10^{-3} \text{ M}_\odot \text{ yr}^{-1}$ until it reaches a mass of 2775 M_\odot at the end of the run at 719 kyr . In H2 radiation from the central star terminates its growth 250 kyr after formation at a mass of 1770 M_\odot . But another star forms at 100 kyr and grows through mergers with other star particles and accretion until it reaches a mass of 8670 M_\odot at the end of the simulation at 354 kyr . The two stars produce the highly anisotropic H II region visible at 354 kyr in Figure 3.

The star in H3 initially grows faster than those in the other haloes, with peak accretion rates of $0.03 \text{ M}_\odot \text{ yr}^{-1}$ over the first 20 kyr . The large drop in rate at about 100 kyr is due to strong radiatively-driven outflows. The mass of the star at the end of the run is 2743 M_\odot , having accreted at an average rate of $0.003 \text{ M}_\odot \text{ yr}^{-1}$. Average accretion rates for the main star in H4 are similar, $\sim 0.003 \text{ M}_\odot \text{ yr}^{-1}$, and it reaches a mass of 2638 M_\odot 880 kyr after formation. The sharp dips in rate at 400 kyr and 850 kyr correspond to strong outflows that drive dense gas away from the star, the latter of which is visible in the temperature image at 880 kyr in Figure 3. In H5 and H6, the initial growth of the stars is comparable to those in the other haloes but at 270 kyr and 400 kyr the H II region breaks out of the disk and accretion onto the stars plummets. The final mass of the central star in H5 and H6 is 2079 M_\odot and 1955 M_\odot , respectively.

Overall, accretion onto the stars is intermittent and falls by a few orders in magnitude during outflows. The most massive stars are $1700 - 2800 \text{ M}_\odot$ and, given the flattening in all the mass profiles, are unlikely to grow beyond a few thousand solar masses. This is true of the stars in H1 and H4, which were evolved for twice as long as the others (719 kyr and 880 kyr , respectively) but grew in mass by less than a factor of two after their profiles flattened out. The second most massive stars have typical masses of about 100 M_\odot , are born in the last $100 - 200 \text{ kyr}$ and have accretion rates of $\sim 0.001 \text{ M}_\odot \text{ yr}^{-1}$. The masses of all stars in our simulations are listed in Table 1.

The maximum resolution in our simulation is 300 AU so we cannot resolve protostellar disks around individual stars. However,

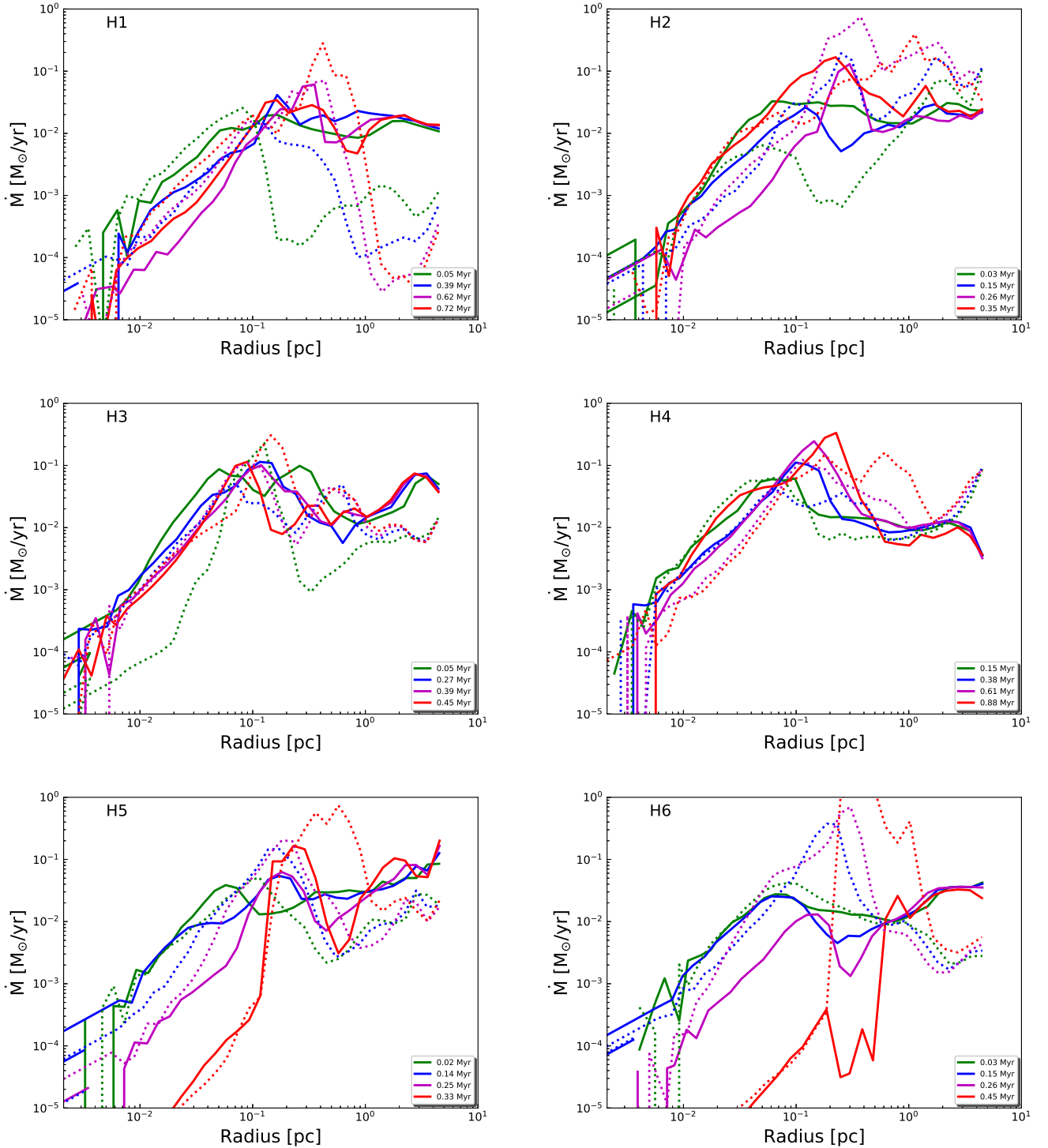


Figure 4. Spherically averaged gas inflow and outflow rates in radial shells centered on the the most massive star in each halo. Solid lines are inflow rates and dotted lines are outflow rates. Upper left: H1, 100 J_{21} ; upper right: H4, 500 J_{21} ; center left: H2, 100 J_{21} ; center right: H5, 500 J_{21} ; bottom left: H3, 100 J_{21} ; bottom right: H6, 500 J_{21} .

even if fragmentation occurs on smaller scales the clump migration timescale is shorter than the Kelvin-Helmholtz timescale at higher densities. Clumps are therefore expected to migrate inwards and merge with the central object (Latif & Schleicher 2015). We resimulated H1 with a maximum spatial resolution of 75 AU (four times

that of the others) and found that the most massive star grew to 600 M_{\odot} in 57 kyr. As shown in Figure 6, its accretion rate and growth track are quite similar to those in the original run so our results likely hold at even higher resolution.

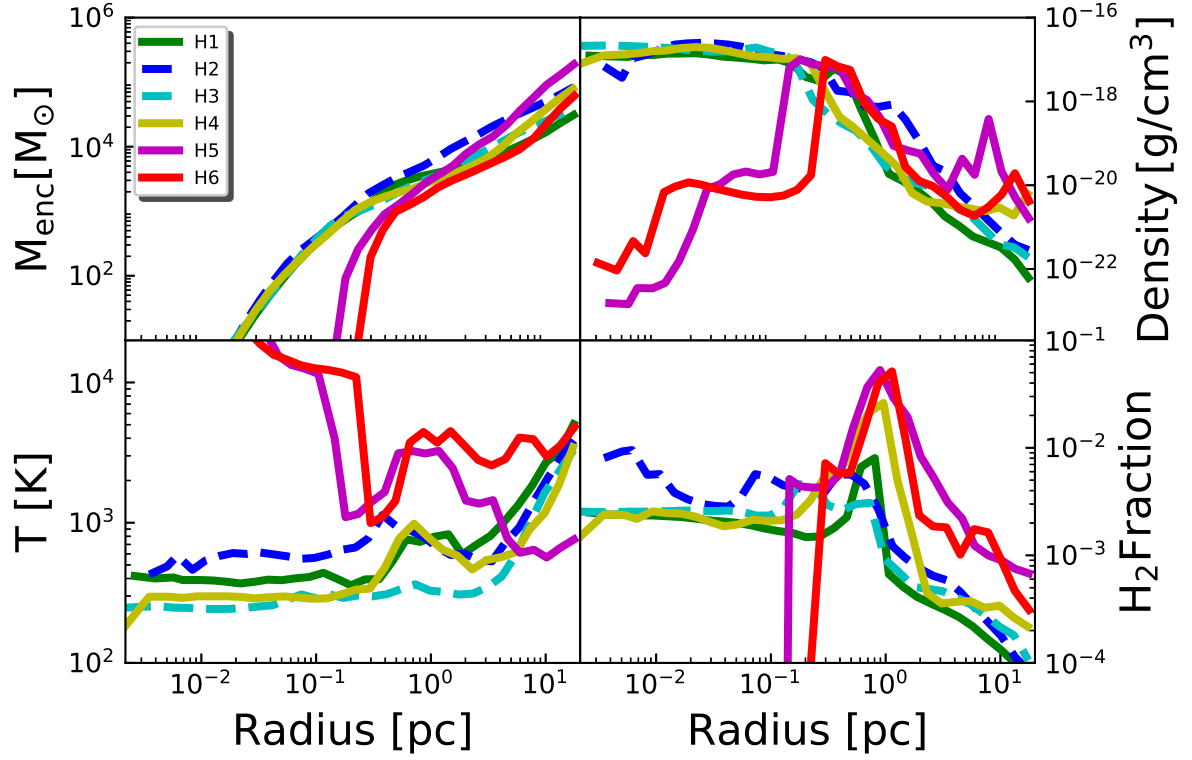


Figure 5. Spherically-averaged densities, temperatures, enclosed masses and H_2 mass fractions at the end of each run. Green, blue, cyan, yellow, magenta and red colors are H1, H2, H3, H4, H5, and H6, respectively.

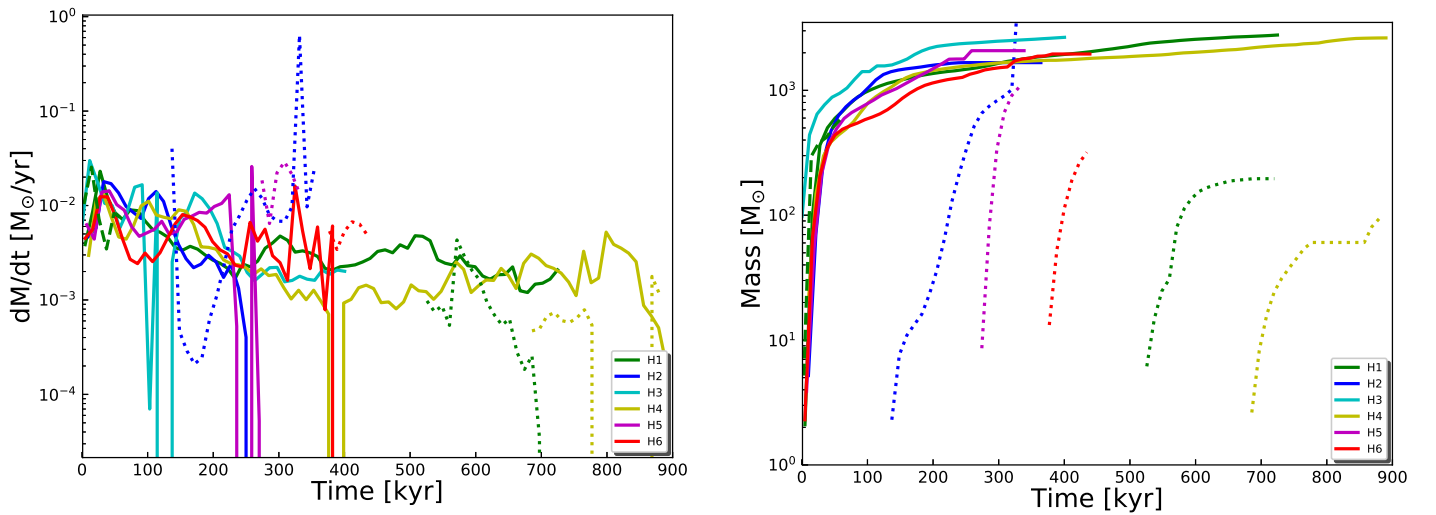


Figure 6. Accretion rates and masses of the two most massive stars in each halo. The green, blue, cyan, yellow, magenta and red lines are H1, H2, H3, H4, H5, and H6, respectively. The solid lines are for the most massive stars and the dotted lines are for the second most massive star. The dashed green line is for H1 at a resolution of 75 AU evolved to 57 kyr.

4 DISCUSSION AND CONCLUSION

We find that moderate LW backgrounds in the primordial universe led to the formation of 1000 - 5000 M_{\odot} Pop III stars, intermediate in mass to those in minihaloes before such backgrounds existed (30 - 500 M_{\odot} ; Hirano et al. 2014, 2015) and those in atomically-cooled haloes in the most extreme backgrounds ($\sim 10^5 M_{\odot}$; e.g. Woods et al. 2017). Intermediate LW backgrounds enabled primordial haloes to grow to somewhat larger masses before forming stars while allowing some H_2 to survive in their cores. This led to a more massive gas reservoir in the center of the halo that was at higher temperatures than those normally associated with H_2 cooling. At the onset of collapse, $Ly\alpha$ cooling dominated in the outer regions of the halo but H_2 cooling regulated the collapse of the core, but at rates that were 10 - 50 times higher than those in minihaloes because the higher virial temperatures were close to the peak in the H_2 cooling and formation rates. Supercharged H_2 cooling thus produced 1000 - 5000 M_{\odot} Pop III stars. We find that fragmentation in haloes in moderate LW backgrounds tends to be mild so these stars are usually accompanied by a few normal Pop III stars. Because such backgrounds were likely common at high redshifts (Agarwal et al. 2014), they opened a third channel of Pop III SF that led to the birth intermediate mass black holes in primordial galaxies.

Although stellar evolution calculations would be required to know for certain how long our simulations would have to be run to for our stars to collapse to BHs (and what their masses would be), it is probable that they would be less than twice the final masses of the stars in our runs. Our longest simulations were evolved for more than half the expected lifetimes of the stars they produce (Schaerer 2002) and radiative feedback levels off their masses well before the end of the runs. Our stars are not massive enough to encounter the GR instability, which usually happens at a few $10^4 M_{\odot}$, so they would likely collapse via the photodisintegration instability (Heger & Woosley 2002; Heger et al. 2003) or He depletion in the core without exploding (see Figure 4 of Woods et al. 2020).

We find that radiation from the star plays a pivotal role in its evolution in intermediate LW backgrounds. Accretion rates in haloes collapsing via $Ly\alpha$ and H_2 cooling can be 100 times lower than those cooling by $Ly\alpha$ alone, and are close to the limit below which the stars become blue and hot rather than cool and red ($0.001 - 0.01 M_{\odot} \text{ yr}^{-1}$; Haemmerlé et al. 2018a). Thus, if a star happens to be born blue in such a halo its ionizing UV radiation tends to keep it blue by curtailing accretion onto it. As the star becomes more massive it becomes more luminous and drives accretion rates even lower. None of the stars in our runs ever become red because they never reach accretion rates of $0.04 M_{\odot} \text{ yr}^{-1}$. This rate is larger than those found in stellar evolution models to cause stars to become blue so the radiative feedback in our models should be taken to be an upper limit and the true masses of the stars may be somewhat higher.

Our results are generally consistent with previous studies that found fragmentation in massive primordial halos in moderate LW fields (Safranek-Shrader et al. 2012; Latif et al. 2014c; Regan & Downes 2018b). We note that Regan & Downes (2018b) considered a single halo at several resolutions and LW backgrounds of 1, 100 and 1000 J_{21} for 250 kyr (and 500 kyr in two cases). Our study differs from Regan & Downes (2018b) in two important ways: we modeled six haloes that enable us to study variations from halo to halo and followed accretion onto the stars for up to 900 kyr, 4 times longer. The most massive star in our runs is a factor of a few lower in mass than that in Regan & Downes (2018b), most likely because all of our stars were taken to be blue and hot, and therefore

significant sources of radiative feedback. Stellar feedback generates outflows in our simulations on parsec scales and quenches inflows from larger scales.

Less fragmentation occurs in our models than in simulations of normal Pop III star formation (Turk et al. 2009; Clark et al. 2011; Greif et al. 2012; Susa et al. 2014; Latif & Schleicher 2015; Stacy et al. 2016; Hosokawa et al. 2016; Susa 2019; Sugimura et al. 2020). Even though SF in our haloes is also regulated by H_2 cooling, the gas at the center of the disk is several times hotter so it is better supported by thermal pressure against fragmentation. Regan & Downes (2018b) find somewhat more fragmentation than we do in part because of higher resolution but, as noted earlier, the ultimate fates of these fragments is not known as some will likely merge at later times. In reality, most simulations of atomic collapse performed to date probably overestimate fragmentation because they ignore magnetic fields that likely arose in most primordial haloes because of subgrid turbulent dynamos (Schober et al. 2012; Turk et al. 2012; Latif et al. 2013a, 2014a; Sharda et al. 2020). Such fields would tend to stabilize the disk and suppress fragmentation.

Even though the central Pop III stars become very massive and luminous by the end of our runs it is unlikely that they will be visible to future surveys by the *James Webb Space Telescope* (*JWST*), ground-based extremely-large telescopes (ELTs), *Euclid*, or the *Roman Space Telescope* (*RST*). All flux blueward of the Lyman limit in the rest frame of the star is absorbed by the neutral intergalactic medium prior to the end of cosmological reionization, so only cosmologically-redshifted flux redward of this limit could be observed. Taking into account reprocessing of stellar flux by their dense, atomically-cooled envelopes, Surace et al. (2018, 2019) found that red and blue $10^5 M_{\odot}$ stars would be only marginally detectable in wide fields by *Euclid* or the *RST* at $z \sim 6 - 8$, and they are a few orders of magnitude brighter than the stars in our models. They found that *JWST* could detect such stars at somewhat higher redshifts but only if one happened to appear in its narrow field of view.

Although stellar evolution models of 1000 - 5000 Pop III M_{\odot} stars only sparsely cover this mass range, they predict collapse to BHs without explosions. They are less likely to explode than cool red stars of equal mass because they are more compact and therefore more deeply gravitationally bound objects. Less massive secondary stars in their orbit could die as pair-instability supernovae (PI SNe) that could be detected in future surveys (e.g., Whalen et al. 2013a,b; de Souza et al. 2013, 2014; Hartwig et al. 2018b; Moriya et al. 2019) but these events would not mark the presence of a much more massive star in the same halo because less-massive minihaloes are also predicted to produce 140 - 260 M_{\odot} Pop III stars. However, secondary stars in highly eccentric orbits with the central star could produce tidal disruption events (TDEs) if they are torn apart after the main star collapses to a BH (Kashiyama & Inayoshi 2016). The mass ratios of the two stars are distinct from those of more massive DCBHs and tightly clustered stars in higher LW backgrounds and could produce near infrared (NIR) signatures that are unique to this Pop III star formation channel.

Because DCBHs have been found to be just above detection thresholds at $z \sim 15 - 20$ for *JWST* in the NIR it is unlikely that the stars in our simulations could be observed after collapsing to BHs because they would be 20 - 50 times less massive (Pacucci et al. 2015; Natarajan et al. 2017; Whalen et al. 2020b). Detections in the radio would be even more difficult because more massive DCBHs at this epoch will only be marginally visible to the Square Kilometre Array (SKA) or next-generation Very Large Array (ngVLA);

Whalen et al. 2020a,b). However, gravitational waves (GWs) from mergers between the main stars in our models and the secondary stars orbiting them might be detectable by the Laser Interferometry Space Antenna (LISA; Hartwig et al. 2018a). Their mass ratios could again distinguish them from mergers between more DCBHs.

It is not clear if the extremely massive Pop III stars in our simulations could later evolve into the first quasars because Smidt et al. (2018) found that they must be seeded by BHs of at least $10^5 M_\odot$ at $z \sim 20$ to reach $10^9 M_\odot$ by $z \sim 7$ in the cold accretion flows that are thought to fuel their growth (see also Latif & Khochfar 2020). If not, they could instead yield a population of less-massive, lower-luminosity quasars that are yet to be discovered. Synergies between *JWST* and *Euclid* or the *RST* could reveal the existence of these objects when they inaugurate the era of $5 < z < 15$ quasar astronomy in the coming decade.

ACKNOWLEDGEMENTS

MAL thanks the UAEU for funding via UPAR grant No. 31S390. DRGS thanks for funding via the Chilean BASAL Centro de Excelencia en Astrofísica y Tecnologías Afines (CATA) grant PFB-06/2007.

5 DATA AVAILABILITY STATEMENT

The data underlying this article will be shared on reasonable request to the corresponding author.

REFERENCES

- Abel T., Anninos P., Zhang Y., Norman M. L., 1997, *New Astronomy*, **2**, 181
- Agarwal B., Khochfar S., 2015, *MNRAS*, **446**, 160
- Agarwal B., Dalla Vecchia C., Johnson J. L., Khochfar S., Paardekooper J.-P., 2014, *MNRAS*, **443**, 648
- Agarwal B., Cullen F., Khochfar S., Ceverino D., Klessen R. S., 2019, *MNRAS*, **488**, 3268
- Alvarez M. A., Wise J. H., Abel T., 2009, *ApJ*, **701**, L133
- Ardaneh K., Luo Y., Shlosman I., Nagamine K., Wise J. H., Begelman M. C., 2018, *MNRAS*, **479**, 2277
- Bañados E., et al., 2018, *Nature*, **553**, 473
- Becerra F., Greif T. H., Springel V., Hernquist L. E., 2015, *MNRAS*, **446**, 2380
- Becerra F., Marinacci F., Bromm V., Hernquist L. E., 2018, *MNRAS*, **480**, 5029
- Boekholt T. C. N., Schleicher D. R. G., Fellhauer M., Klessen R. S., Reinoso B., Stutz A. M., Haemmerlé L., 2018, *MNRAS*, **476**, 366
- Bromm V., Loeb A., 2003, *ApJ*, **596**, 34
- Bryan G. L., et al., 2014, *ApJS*, **211**, 19
- Chon S., Hosokawa T., Yoshida N., 2018, *MNRAS*, **475**, 4104
- Clark P. C., Glover S. C. O., Smith R. J., Greif T. H., Klessen R. S., Bromm V., 2011, *Science*, **331**, 1040
- Devecchi B., Volonteri M., 2009, *ApJ*, **694**, 302
- Greif T. H., White S. D. M., Klessen R. S., Springel V., 2011, *ApJ*, **736**, 147
- Greif T. H., Bromm V., Clark P. C., Glover S. C. O., Smith R. J., Klessen R. S., Yoshida N., Springel V., 2012, *MNRAS*, **424**, 399
- Haemmerlé L., Woods T. E., Klessen R. S., Heger A., Whalen D. J., 2018a, *MNRAS*, **474**, 2757
- Haemmerlé L., Woods T. E., Klessen R. S., Heger A., Whalen D. J., 2018b, *ApJ*, **853**, L3
- Hahn O., Abel T., 2011, *MNRAS*, **415**, 2101
- Haiman Z., 2013, in Wiklind T., Mobasher B., Bromm V., eds, *Astrophysics and Space Science Library* Vol. 396, Astrophysics and Space Science Library, p. 293 ([arXiv:1203.6075](https://arxiv.org/abs/1203.6075)), doi:10.1007/978-3-642-32362-1_6
- Hartwig T., Agarwal B., Regan J. A., 2018a, *MNRAS*, **479**, L23
- Hartwig T., Bromm V., Loeb A., 2018b, *MNRAS*, **479**, 2202
- Heger A., Woosley S. E., 2002, *ApJ*, **567**, 532
- Heger A., Fryer C. L., Woosley S. E., Langer N., Hartmann D. H., 2003, *ApJ*, **591**, 288
- Hirano S., Hosokawa T., Yoshida N., Umeda H., Omukai K., Chiaki G., Yorke H. W., 2014, *ApJ*, **781**, 60
- Hirano S., Hosokawa T., Yoshida N., Omukai K., Yorke H. W., 2015, *MNRAS*, **448**, 568
- Hosokawa T., Yorke H. W., Inayoshi K., Omukai K., Yoshida N., 2013, *ApJ*, **778**, 178
- Hosokawa T., Hirano S., Kuiper R., Yorke H. W., Omukai K., Yoshida N., 2016, *ApJ*, **824**, 119
- Inayoshi K., Visbal E., Haiman Z., 2019, *arXiv e-prints*, p. [arXiv:1911.05791](https://arxiv.org/abs/1911.05791)
- Johnson J. L., Whalen D. J., Li H., Holz D. E., 2013, *ApJ*, **771**, 116
- Kashiyama K., Inayoshi K., 2016, *ApJ*, **826**, 80
- Latif M. A., Ferrara A., 2016, *Publ. Astron. Soc. Australia*, **33**, e051
- Latif M. A., Khochfar S., 2019, *MNRAS*, **490**, 2706
- Latif M. A., Khochfar S., 2020, *MNRAS*, **497**, 3761
- Latif M. A., Schleicher D. R. G., 2015, *MNRAS*, **449**, 77
- Latif M. A., Volonteri M., 2015, *MNRAS*, **452**, 1026
- Latif M. A., Schleicher D. R. G., Schmidt W., Niemeyer J., 2013a, *MNRAS*, **432**, 668
- Latif M. A., Schleicher D. R. G., Schmidt W., Niemeyer J., 2013b, *MNRAS*, **433**, 1607
- Latif M. A., Schleicher D. R. G., Schmidt W., Niemeyer J., 2013c, *ApJ*, **772**, L3
- Latif M. A., Schleicher D. R. G., Schmidt W., 2014a, *MNRAS*, **440**, 1551
- Latif M. A., Bovino S., Van Borm C., Grassi T., Schleicher D. R. G., Spaans M., 2014b, *MNRAS*, **443**, 1979
- Latif M. A., Schleicher D. R. G., Bovino S., Grassi T., Spaans M., 2014c, *ApJ*, **792**, 78
- Latif M. A., Bovino S., Grassi T., Schleicher D. R. G., Spaans M., 2015, *MNRAS*, **446**, 3163
- Latif M. A., Khochfar S., Whalen D., 2020, *ApJ*, **892**, L4
- Luo Y., Ardaneh K., Shlosman I., Nagamine K., Wise J. H., Begelman M. C., 2018, *MNRAS*, **476**, 3523
- Madau P., Haardt F., Dotti M., 2014, *ApJ*, **784**, L38
- Mirocha J., Skory S., Burns J. O., Wise J. H., 2012, *ApJ*, **756**, 94
- Moriya T. J., Wong K. C., Koyama Y., Tanaka M., Oguri M., Hilbert S., Nomoto K., 2019, *PASJ*,
- Mortlock D. J., et al., 2011, *Nature*, **474**, 616
- Natarajan P., Pacucci F., Ferrara A., Agarwal B., Ricarte A., Zackrisson E., Cappelluti N., 2017, *ApJ*, **838**, 117
- O’Shea B. W., Norman M. L., 2007, *ApJ*, **654**, 66
- Pacucci F., Ferrara A., Volonteri M., Dubus G., 2015, *MNRAS*, **454**, 3771
- Patrick S., Whalen D. J., Elford J., Latif M., 2020, *MNRAS*, submitted
- Planck Collaboration et al., 2016, *A&A*, **594**, A13
- Regan J. A., Downes T. P., 2018a, *MNRAS*, **475**, 4636
- Regan J. A., Downes T. P., 2018b, *MNRAS*, **478**, 5037
- Regan J. A., Haehnelt M. G., 2009, *MNRAS*, **393**, 858
- Regan J. A., Johansson P. H., Wise J. H., 2014, *ApJ*, **795**, 137
- Regan J. A., Wise J. H., Woods T. E., Downes T. P., O’Shea B. W., Norman M. L., 2020, *arXiv e-prints*, p. [arXiv:2008.08090](https://arxiv.org/abs/2008.08090)
- Reinoso B., Schleicher D. R. G., Fellhauer M., Klessen R. S., Boekholt T. C. N., 2018, *A&A*, **614**, A14
- Ricotti M., Gnedin N. Y., Shull J. M., 2001, *ApJ*, **560**, 580
- Safranek-Shrader C., Agarwal M., Federrath C., Dubey A., Milosavljević M., Bromm V., 2012, *MNRAS*, **426**, 1159
- Sakurai Y., Yoshida N., Fujii M. S., Hirano S., 2017, *MNRAS*, **472**, 1677
- Schaerer D., 2002, *A&A*, **382**, 28
- Schauer A. T. P., Regan J., Glover S. C. O., Klessen R. S., 2017, *MNRAS*, **471**, 4878
- Schleicher D. R. G., Palla F., Ferrara A., Galli D., Latif M., 2013, *A&A*, **558**, A59
- Schober J., Schleicher D., Federrath C., Glover S., Klessen R. S., Banerjee R., 2012, *ApJ*, **754**, 99

- Sharda P., Federrath C., Krumholz M. R., 2020, *MNRAS*, **497**, 336
- Smidt J., Whalen D. J., Johnson J. L., Surace M., Li H., 2018, *ApJ*, **865**, 126
- Smith A., Becerra F., Bromm V., Hernquist L., 2017, *MNRAS*, **472**, 205
- Smith B. D., Regan J. A., Downes T. P., Norman M. L., O’Shea B. W., Wise J. H., 2018, *MNRAS*, **480**, 3762
- Stacy A., Bromm V., Loeb A., 2011, *ApJ*, **730**, L1
- Stacy A., Bromm V., Lee A. T., 2016, *MNRAS*, **462**, 1307
- Suazo M., Prieto J., Escala A., Schleicher D. R. G., 2019, *ApJ*, **885**, 127
- Sugimura K., Omukai K., Inoue A. K., 2014, *MNRAS*, **445**, 544
- Sugimura K., Matsumoto T., Hosokawa T., Hirano S., Omukai K., 2020, *ApJ*, **892**, L14
- Surace M., et al., 2018, *ApJ*, **869**, L39
- Surace M., Zackrisson E., Whalen D. J., Hartwig T., Glover S. C. O., Woods T. E., Heger A., Glover S. C. O., 2019, *MNRAS*, **488**, 3995
- Susa H., 2019, *ApJ*, **877**, 99
- Susa H., Hasegawa K., Tominaga N., 2014, *ApJ*, **792**, 32
- Tselikhovich D., Hirata C., 2010, *Phys. Rev. D*, **82**, 083520
- Turk M. J., Abel T., O’Shea B., 2009, *Science*, **325**, 601
- Turk M. J., Oishi J. S., Abel T., Bryan G. L., 2012, *ApJ*, **745**, 154
- Umeda H., Hosokawa T., Omukai K., Yoshida N., 2016, *ApJ*, **830**, L34
- Volonteri M., 2010, *A&ARv*, **18**, 279
- Volonteri M., Silk J., Dubus G., 2015, *ApJ*, **804**, 148
- Whalen D. J., Fryer C. L., 2012, *ApJ*, **756**, L19
- Whalen D., Norman M. L., 2008, *ApJ*, **673**, 664
- Whalen D., Abel T., Norman M. L., 2004, *ApJ*, **610**, 14
- Whalen D. J., Fryer C. L., Holz D. E., Heger A., Woosley S. E., Stiavelli M., Even W., Frey L. H., 2013a, *ApJ*, **762**, L6
- Whalen D. J., et al., 2013b, *ApJ*, **777**, 110
- Whalen D. J., Mezcuca M., Meiksin A., Hartwig T., Latif M. A., 2020a, *ApJ*, **896**, L45
- Whalen D. J., Surace M., Bernhardt C., Zackrisson E., Pacucci F., Ziegler B., Hirschmann M., 2020b, *ApJ*, **897**, L16
- Wise J. H., Abel T., 2011, *MNRAS*, **414**, 3458
- Wise J. H., Turk M. J., Abel T., 2008, *ApJ*, **682**, 745
- Wolcott-Green J., Haiman Z., Bryan G. L., 2011, *MNRAS*, **418**, 838
- Woods T. E., Heger A., Whalen D. J., Haemmerlé L., Klessen R. S., 2017, *ApJ*, **842**, L6
- Woods T. E., et al., 2019, *Publ. Astron. Soc. Australia*, **36**, e027
- Woods T. E., Heger A., Haemmerlé L., 2020, *MNRAS*, **494**, 2236
- Wu X.-B., et al., 2015, *Nature*, **518**, 512
- Yang J., et al., 2020, *ApJ*, **897**, L14
- de Souza R. S., Ishida E. E. O., Johnson J. L., Whalen D. J., Mesinger A., 2013, *MNRAS*, **436**, 1555
- de Souza R. S., Ishida E. E. O., Whalen D. J., Johnson J. L., Ferrara A., 2014, *MNRAS*, **442**, 1640

This paper has been typeset from a \LaTeX file prepared by the author.